Fundamental Study on the Modeling of Flame Propagation in Constant Volume Vessels

Michikata Kono and Tatsuro Tsukamoto
Department of Aeronautics, Faculty of Engineering, University of Tokyo, Bunkyo-ku, Tokyo

Kazuo Iinuma
Department of Mechanical Engineering, Hosei University, Koganei, Tokyo

ABSTRACT

From the fundamental point of view with reference to the combustion simulation in SI engines by using unsteady multi-dimensional model, one- and two-dimensional models were employed on the flame propagation in the constant volume vessels under room temperature and atmospheric pressure condition. The validity of the one-dimensional spherical coordinate model is well confirmed by the experiment on the flame propagation within a spherical combustion chamber. However, two-dimensional rectangubar coordinate model used was found to be not so effective for the simulation of the flame propagation in a cylindrical combustion chamber with central ignition. From those results, it is suggested that the heat loss to the wall of the combustion chamber is of importance and this may be evaluated correctly by a three-dimensional model.

INTRODUCTION

Recently, combustion simulation of SI engines is frequently tried by unsteady multi-dimensional model in order to clarify or deeply understand the mechanism of the engine combustion and to enhance the engine performance from the designing point of view (1, 2). However, to the authors' knowledge, it is not so easy to utilize such simulation model properly under a given condition, which is due not only to computing time and cost, or computing procedure and the accuracy of the results, but also to the complicated process of the flame propagation. The process includes the chemical reaction, heat loss to the chamber wall, turbulence effect, effect of flow field before and after ignition, and complicated chamber geometry. Therefore, it is important, step by step, to examine the individual process included in the flame propagation process.

In the present work, from the fundamental point of view, one- and two-dimensional models on the flame propagation were developed under laminar flow condition. First, one-dimensional modeling was developed for spherical flame propagation. Its result was compared with that of experiment, and then the optimum values of the several parameters included in the model were decided. Finally, by using these values of the parameters, the validity of the two-dimensional model simulating the flame propagation in a cylindrical combustion chamber was evaluated.

SPHERICAL ONE-DIMENSIONAL MODEL

Model Description

In a spherical vessel which is filled with propane-air mixture, a certain spherical flame kernel is assumed to be placed initially at its center. The flame kernel is to be able to develop into a self-sustained flame, which spherically propagates outward under laminar flow condition. Such flame propagation is simulated by a set of unsteady partial differential equations based on the spherical and radial one-dimensional coordinate. Buoyancy effect, heat transfer by radiation and diffusion by temperature gradient are neglected due to their smaller value comparing with other parameters.

Fundamental Equations

The partial differential equations used are as follows:

Mass conservation.

$$\frac{\partial \rho}{\partial t} + \frac{1}{r^2}\frac{\partial \rho u r^2}{\partial r} = 0 \tag{1}$$

Momentum conservation.

$$\frac{\partial \rho u}{\partial t} + \frac{1}{r^2}\frac{\partial \rho u^2 r^2}{\partial r} = -\frac{\partial p}{\partial r} + \frac{1}{r^2}\frac{\partial \sigma_{rr} r^2}{\partial r} - \frac{\sigma_{\theta\theta}+\sigma_{\phi\phi}}{r} \tag{2}$$

Energy conservation.

$$\frac{\partial e_t u}{\partial t} + \frac{1}{r^2}\frac{\partial \rho e_t u r^2}{\partial r} = -\frac{1}{r^2}\frac{\partial p u r^2}{\partial r} + \frac{1}{r^2}\frac{\partial \sigma_{rr} u r^2}{\partial r} - \frac{1}{r^2}\frac{\partial q_r r^2}{\partial r} + \dot{q}_c \tag{3}$$

Species conservation.

$$\frac{\partial \rho_i}{\partial t} + \frac{1}{r^2}\frac{\partial \rho_i u r^2}{\partial r} = \frac{1}{r^2}\frac{\partial}{\partial r}\left(r^2 \rho D \frac{\partial Y_i}{\partial r}\right) + (\dot{\rho}_i)_c \tag{4}$$

Equation of state.

$$p = \rho RT \tag{5}$$

In these equations, relations between viscous stress and rates of strain, the energy flux, q_r, the specific total energy, e_t, and the enthalpy are given as:

$$\sigma_{rr} = 2\mu\frac{\partial u}{\partial r} + \lambda\frac{1}{r^2}\frac{\partial ur^2}{\partial r} \tag{6}$$

$$\sigma_{\theta\theta} = \sigma_{\phi\phi} = 2\mu\frac{u}{r} + \lambda\frac{1}{r^2}\frac{\partial ur^2}{\partial r} \tag{7}$$

$$q_r = -\kappa\frac{\partial T}{\partial r} - \sum_{i=1}^{n} \rho_i hD\frac{\partial Y_i}{\partial r} \tag{8}$$

$$e_t = e + \frac{1}{2}u^2 \tag{9}$$

$$h = e + \frac{p}{\rho} \tag{10}$$

where λ is taken as $-2/(3\mu)$.

The diffusion coefficient is assumed to be independent of temperature, pressure and species concentration. Prandtl and Lewis numbers are assumed to be unity, and therefore the following relations are obtained.

$$\kappa = DC_p\rho \tag{11}$$

$$\mu = D\rho \tag{12}$$

For simplicity, chemical species were assumed to be propane, oxygen, nitrogen and combustion product, so that the heat releasing reaction is represented by a one-step irreversible equation as follows:

$$C_3H_8 + 5O_2 + 18.8N_2 \xrightarrow{k} 7\text{Product} + 18.8N_2 + Q, \tag{13}$$

where the molecular mass of the product can be obtained as 29.1. The reaction rate constant k is assumed to be Arrhenius type as:

$$k = A\exp(-E/\bar{R}T). \tag{14}$$

The reaction rate can be given as

$$\omega = k\,(\rho_{C_3H_8}/M_{C_3H_8})^a(\rho_{O_2}/M_{O_2})^b. \tag{15}$$

Eqs. (13)-(15) give next relations.

$$\dot{q}_c = Q\omega \quad (16), \qquad (\dot{\rho}_{C_3H_8})_c = -M_{C_3H_8}\omega \quad (17)$$

$$(\dot{\rho}_{O_2})_c = -5M_{O_2}\omega \quad (18), \qquad (\dot{\rho}_{N_2})_c = 0 \quad (19)$$

$$(\dot{\rho}_{Prod.})_c = 7M_{Prod.}\omega \quad (20)$$

Temperature dependence of the specific heats was introduced after Gupta et al. (1).

$$e = \sum_{i=1}^{n} Y_i e_i = \sum_{i=1}^{n} Y_i \int_0^T C_{vi}(T)\,dT \tag{21}$$

$$C_{vi}(T) = C_i C_{vN_2}(T) \tag{22}$$

$$e_{N_2} = \int_0^T C_{vN_2}(T)\,dT \tag{23}$$

$$e = e_{N_2}\sum_{i=1}^{n} Y_i C_i \tag{24}$$

$$C_{vN_2} = 5.43\times10^6 + 5.68\times10^3\,T - 2.47\,T^2 + 3.67\times10^{-4}\,T^3 \tag{25}$$

$$T = 90.3 + 1.28\times10^{-1}\,e_{N_2} - 1.22\times10^{-18}\,e_{N_2}^{\,2} + 11.7\times10^{-29}\,e_{N_2}^{\,3} \tag{26}$$

where C_i=3.2, 1, 1, 1.5 for propane, oxygen, nitrogen and product, respectively.

Numerical Solution

The following set of boundary conditions is used at both the center and wall of the spherical vessel:

$$u = 0 \quad (27), \qquad \frac{\partial T}{\partial r} = 0 \quad (28)$$

$$\frac{\partial \rho_i}{\partial r} = 0 \quad (29)$$

The actual ignition process develops in a rather complicated manner (3, 4) and therefore has not well been understood. In the present work, simulation starts from a flame kernel which is formed over a few computational cells. In each cell, a degree of the reaction progress was designated beforehand; for example, such an obtained temperature profile within the flame kernel can be seen at t = 0 in Fig. 4. The initial condition is assumed as a quiescent, stoichiometric propane-air mixture of atmospheric pressure and 300 K temperature.

Partial differential equations, Eqs. (1)-(4), are solved essentially by the RICE code (5, 6). Simply, the procedure of numerical solution can be expressed as follows at a given time step:

1) T is calculated from Eq. (26)
2) C_v is calculated from Eq. (25), and then C_p.
3) By using Eq. (5), p is obtained.
4) Equations (1) and (2) are solved by an implicit scheme and then ρ and v are calculated.
5) Equation (3) is solved explicitly except for the source term due to chemistry and the enthalpy diffusion term in Eq. (8), so that e_t and e are obtained.
6) From Eq. (4) where $(\dot{\rho}_i)_c$ is deleted, ρ_i is calculated explicitly.
7) e_t and e are corrected by calculating the enthalpy diffusion term in Eq. (8).
8) k is obtained from T calculated by use of Eq. (26), and then ω can be decided. In consequence, Eqs. (16)-(20) can be calculated, and therefore e and e_t, and ρ_i are corrected by $\dot{q}_c$ and $(\dot{\rho}_i)_c$, respectively.

The cell size used is 1 mm and the time step is 0.5 μsec. As the value of Q, the net heat of combustion of propane, 2.045 MJ/mol, was finally used. As regards the chemical reaction rate relating to Eqs. (14) and (15), the effect of pre-exponential factor was preferentially examined, while values of the activation energy, E, and the reaction orders, a and b, were assumed to be 0.125 MJ/mol and 0.5, respectively.

Experiment

In Fig. 1, the structure of spherical

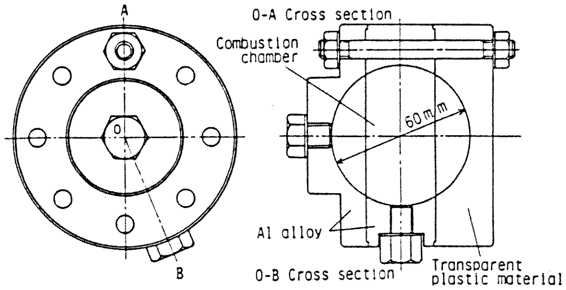

Fig. 1. Spherical combustion chamber.

combustion chamber is shown, whose internal diameter is 60 mm. The combustion chamber consists of three components, namely the central component and a pair of side components. They all are made of Al alloy. When the velocity is measured by Laser Doppler Velocimeter (LDV), both the side components are replaced by those of transparent plastic material, so that laser beam can pass through inside of the combustion chamber and also the scattered-light signal can be received by a photomultiplier located outside the combustion chamber.

After the combustion chamber is filled with a propane-air mixture of stoichiometric ratio, an electric spark, which is supplied by CDI system, is generated at the centrally placed spark gap of 1 mm in gap distance. The position of the flame front was measured by a single ion probe. The ion probe was located at 5, 10, 15, 20 and 25 mm horizontally away from the spark gap. The pressure change in the combustion chamber was measured by the pressure transducer (KISTLER 601H), and the charge amplifier (KISTLER 5007). The output of the charge amplifier, as well as the ion probe signal, was recorded by an oscilloscope equipped with a digital memory.

The velocity change of gas in the combustion chamber was measured by LDV. The measuring system is shown in Fig. 2. The He-Ne laser beam of the light source (NEC GLG5601, 15 mW output, 632.8 nm wave length) is split into two beams, one of which is imposed by an optical frequency shift (0.5 kHz). The two beams are then focussed by the converging lens (240.5 mm focal length, 11.57 degree total angle of beam intersection) into the combustion chamber. The diameter and length of the

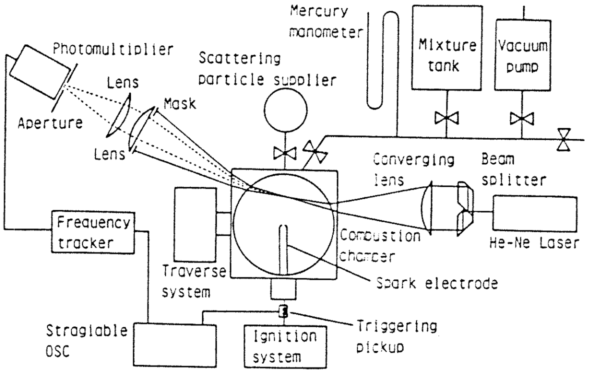

Fig. 2. Schematic diagram of velocity measurement by LDV.

measuring volume formed in the combustion chamber is roughly 50 and 500 μm, respectively. The Doppler signal through the wall of the combustion chamber is collected by a photomultiplier system, the output of which is processed by a frequency tracker (KANOMAX model 1090A). By means of the above system, velocity change against time was measured at 7, 13 and 20 mm from the center of the combustion chamber. Particles of small size (Kanto loam, JIS powder No. 11) were used for laser scattering, which were floated in the mixture just prior to an ignition by using a rubber syringe (Fig. 2).

Comparison of Calculated and Measured Results

As can be seen in the partial differential equations mentioned above, there is a possibility that many parameters affect the calculated results. Especially, the following three ones: the heat of combustion, the reaction rate constant and the diffusion coefficient were found to be predominant, so that effect of these three parameters were examined in the first place. Naturally, as is seen in Eqs. (11) and (12), only

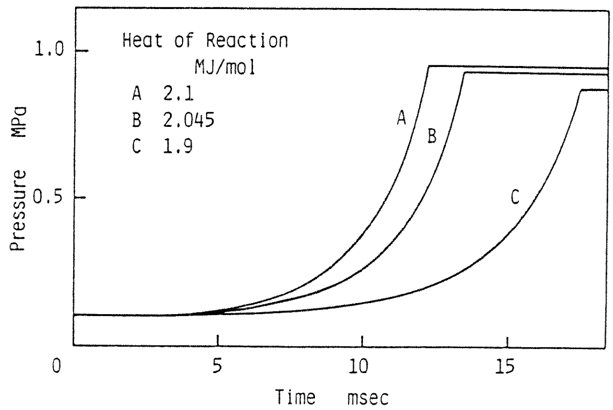

Fig. 3. Calculated pressure vs. time for different heats of combustion. $D = 2.0 \times 10^{-3}$ m^2/sec and $A = 50$ m^3/(mol sec).

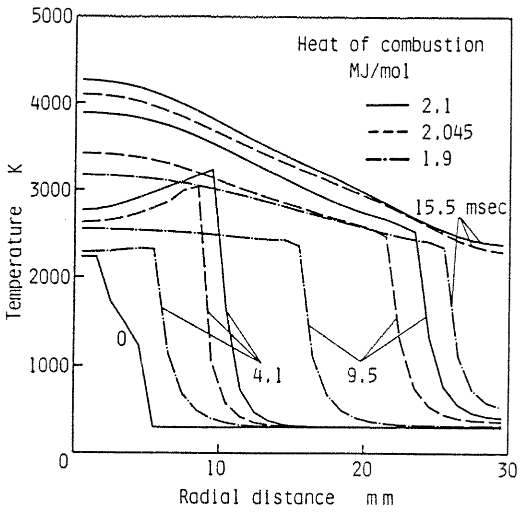

Fig. 4. Temperature distribution for different heats of combustion. $D = 2.0 \times 10^{-3}$ m^2/sec and $A = 50$ m^3/(mol sec).

the diffusion coefficient, D, can not be varied but accordingly $\kappa/C_p\rho$ and μ/ρ change. A preliminary computation revealed that the diffusion coefficient is most effective on the results by using these diffusivities. In order to evaluate the effect of the reaction rate constant, for simplicity, the value of the pre-exponential factor, A, was changed. The calculated results are shown in Figs. 3-8. From these figures, the three parameters mentioned above are found to affect the calculated results namely: the final maximum pressure, p_m, the combustion time, t_c, which is defined as the time when the pressure of the combustion chamber attains to p_m, the thickness of the flame front and the temperature gradient at the flame front. The effect of these parameters can easily be understood by a simple laminar flame theory. Although this theory is not unsteady like the simulation model but is steady, it is sufficient for grasping the essential features of the flame propagation process in the constant volume vessel.

A stationary flame front of thickness δ, into which unburned mixture flows at velocity S_u is assumed as shown in Fig. 9. The mass conservation

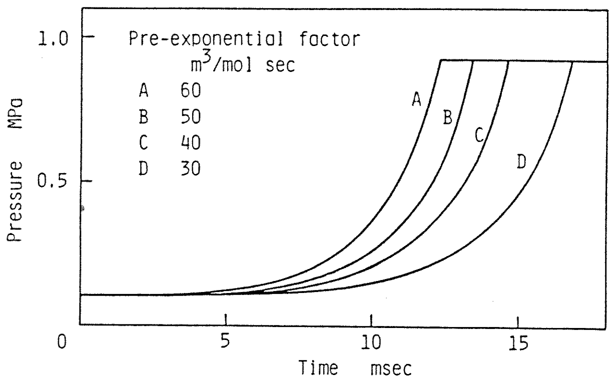

Fig. 5. Calculated pressure vs. time for different pre-exponential factors. Q = 2.045 MJ/mol and D = 2.0×10^{-3} m^2/sec.

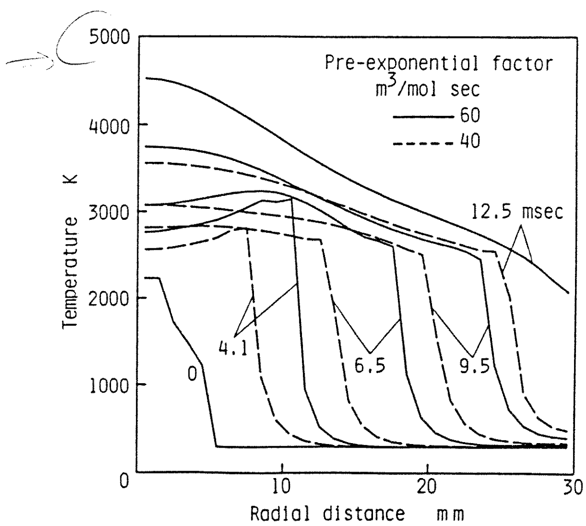

Fig. 6. Temperature distribution for different pre-exponential factors. Q = 2.045 MJ/mol and D = 2.0×10^{-3} m^2/sec.

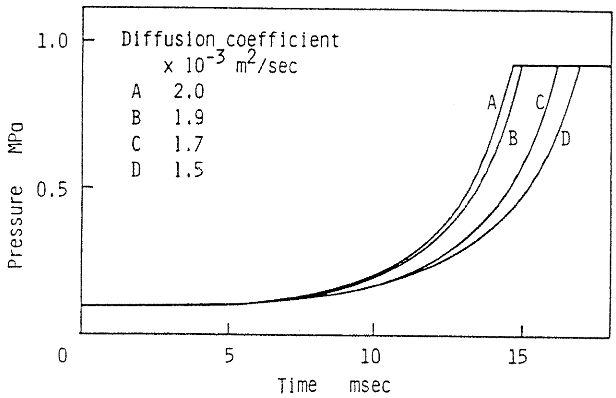

Fig. 7. Calculated pressure vs. time for different diffusion coefficients. Q = 2.045 MJ/mol and A = 40 m^3/(mol sec).

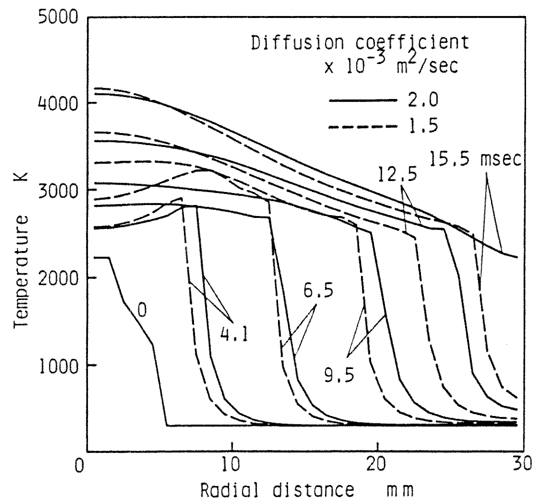

Fig. 8. Temperature distribution for different diffusion coefficients. Q = 2.045 MJ/mol and A = 40 m^3/(mol sec).

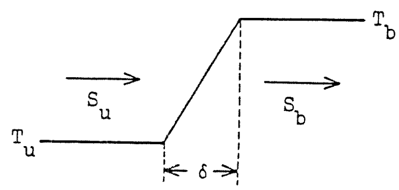

Fig. 9. The structure of flame front.

equation can be obtained as

$$\rho_u S_u = \omega\delta. \tag{30}$$

The energy equation can roughly be expressed as

$$Q\omega\delta = \kappa(T_b - T_u)/\delta, \tag{31}$$

where Q is also expressed as

$$Q = C_p M(T_b - T_u). \tag{32}$$

From Eqs. (31) and (32), the flame thickness is given by

$$\delta = \sqrt{\kappa/(C_p M\omega)}\,. \tag{33}$$

The temperature gradient at the flame front can be obtained by Eqs. (32) and (33) as follows:

$$(T_b - T_u)/\delta = Q\sqrt{\omega/(\kappa C_p M)} \tag{34}$$

The laminar burning velocity, S_u, can be given from Eqs. (30) and (33) as

$$S_u = \sqrt{\kappa\omega/(C_p M)}\,/\rho_u. \tag{35}$$

Furthermore, the continuity equation throughout the flame front is approximately given by $S_u/T_u = S_b/T_b$. Therefore, the velocity of the burned gas relative to the flame fronts, S_b, which contributes to the flame speed to a considerable extent, can be obtained as follows,

$$S_b = S_u T_b/T_u. \tag{36}$$

Naturally, S_b includes the effect of the expansion of the burned gas which pushes the flame front towards the unburned gas. Since in ordinary flames $T_b/T_u >> 1$, T_b/T_u can be written from Eq. (32) as

$$T_b/T_u = Q/(C_p M T_u). \tag{37}$$

Substituting Eqs. (35) and (37) into Eq. (36) leads to the relation:

$$S_b = Q\sqrt{\kappa\omega/(C_p M)^3}\,/(\rho_u T_u), \tag{38}$$

where the combustion time, t_c, is roughly proportional to the reciprocal of S_b; namely

$$t_c \propto 1/S_b. \tag{39}$$

Moreover, the maximum pressure, p_m, is approximately given by

$$p_m = mRT_b/V_c. \tag{40}$$

By substituting Eq. (37) into Eq. (40), one can obtain

$$p_m = QmR/(V_c C_p M). \tag{41}$$

Since $\kappa = \alpha C_p \rho = DC_p\rho$, Eqs. (33), (34), (39) and (41) can be expressed in terms of the three parameters as

$$p_m \propto Q, \tag{42}$$

$$t_c \propto 1/(Q\sqrt{D\omega}), \tag{43}$$

$$\delta \propto \sqrt{D/\omega} \tag{44}$$

and

$$(T_b - T_u)/\delta \propto Q\sqrt{\omega/D}. \tag{45}$$

By these relations of Eqs. (42)-(45), one can fully understand the effect of these parameters which is shown in Figs. 3-8.

As regards the initial condition, the effect of the flame kernel structure was simply examined. An example of the results is shown in Figs. 10 and 11. The calculated flame radius is defined as the radius corresponding to the maximum temperature gradient. Two different temperature profiles in the flame kernel were used for the initial condition which are shown in Fig. 11. In Fig. 10, it is indicated that except for the part in the incipient region, these curves coincide with each other. From this comparison, it is provisionally concluded that if the flame kernel has an only necessary condition for a flame propagation, the

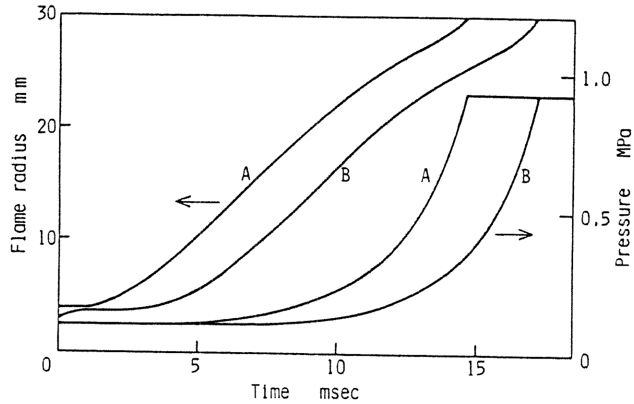

Fig. 10. Calculated flame radius and pressure vs. time for different conditions of flame kernel.

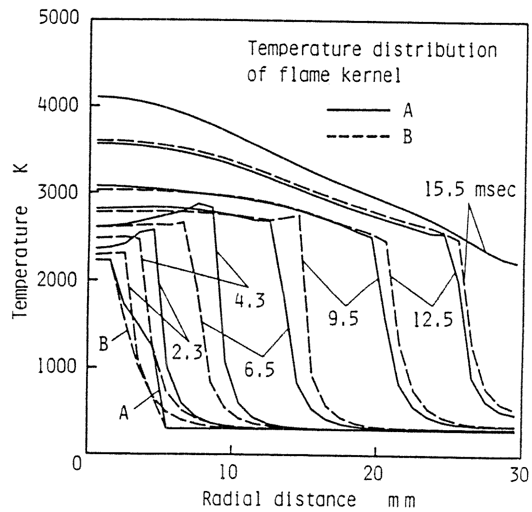

Fig. 11. Temperature distribution for different conditions of flame kernel.

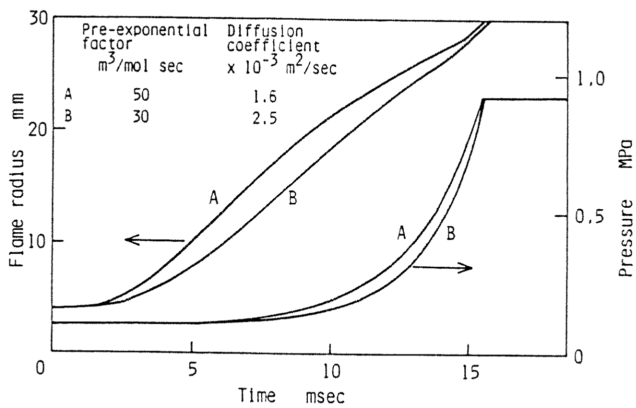

Fig. 12. Calculated flame radius and pressure vs. time for different parameters.

flame kernel structure dose not affect the flame propagation process but the time required for the initiation of the flame propagation.

For the next step towards the excellent calculation, the most reasonable values of these parameters should be selected. As mentioned previously, the net heat of combustion, 2.045 MJ/mol, was used as the value of the heat of combustion, Q. The values of the other parameters, diffusion coefficient and pre-exponential factor, were decided so that the result by calculation best agrees with that by the experiment as follows: In Eq. (43), since Q is constant, the constant value of the product of D and ω gives the constant t_c. An example of the results of such calculation is shown in Fig. 12. As can be seen, the most optimum values of the parameters can be decided by the comparison of the calculated flame radius and pressure change with the experimental results. The optimum values obtained are 40 $m^3/(mol\ sec)$ and $1.9 \times 10^{-3}\ m^2/sec$ for the pre-exponential factor and the diffusion coefficient, respectively.

The result of calculation by using the above-mentioned values of the parameters is shown in

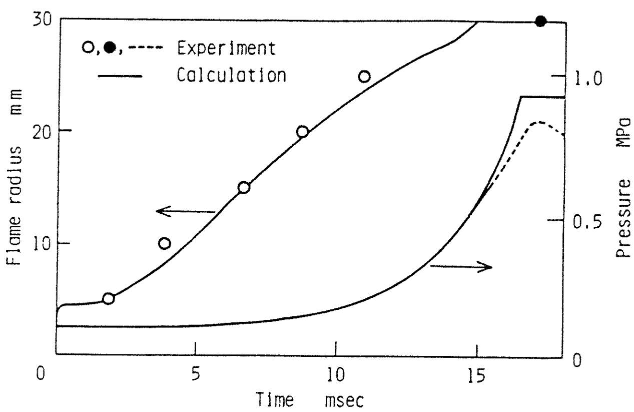

Fig. 13. Flame radius and pressure vs. time. Open circle: ion gap method; solid circle: the maximum pressure point.

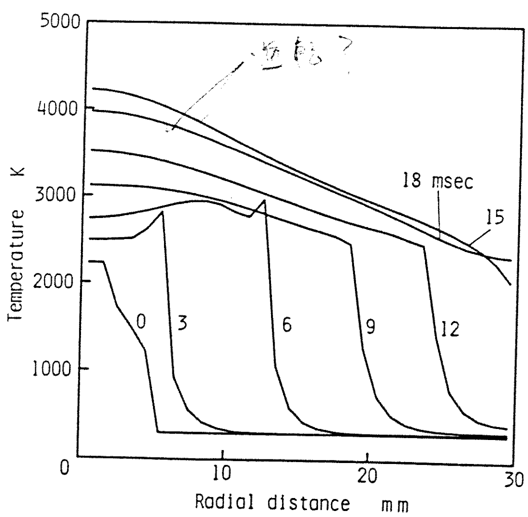

Fig. 14. Temperature distribution calculated by the optimum value of parameters.

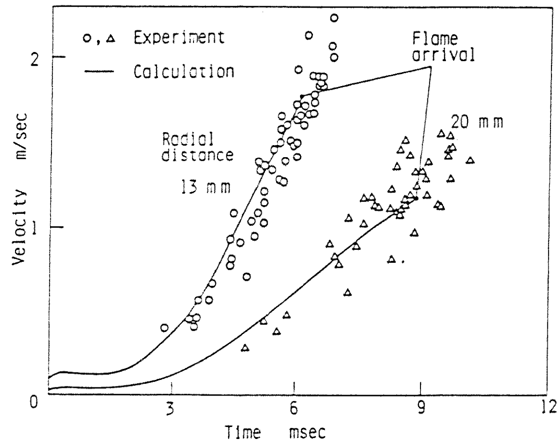

Fig. 15. Velocity change at the point of radial distance of 13 and 20 mm till flame arrival.

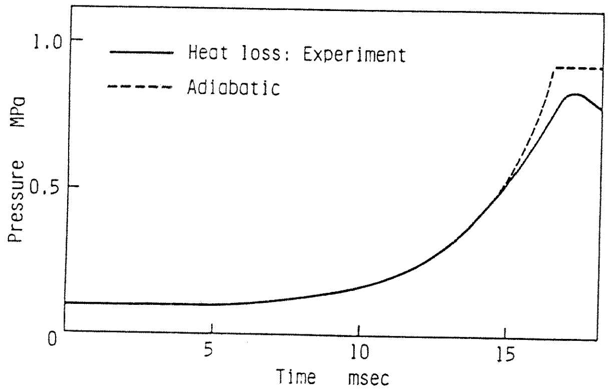

Fig. 16. Pressure vs. time considering the heat loss to the wall. Heat transfer coefficient: 0.6 $MJ/(m^2\ sec\ K)$.

Figs. 13-15. These figures show that the calculated curves of the flame radius, the pressure and the velocity of the unburned gas agree with the experimental results, but it is found that there exists a slight difference at the final stage of the flame propagation. Naturally, the difference is caused by neglecting of heat loss to the wall in the present model. With reference to the pressure curve in Fig. 13, it is shown that about 90% of the total mixture mass burns during the period from 10 to 17 msec, and this burning is found to occur in the thin layer adjacent to the inner wall of the combustion chamber. The thickness of this layer can be read to be about 10 mm from Fig. 14. From this, it is suggested that the heat loss, which affects the combustion in the vicinity of the wall, is of importance for the present model.

In order to consider the effect of heat loss in calculation, it is necessary to assume cells within the wall of the combustion chamber. This procedure requires major change of the computer program. Instead, a heat flux which flows from the most outer cell to the wall is simply included in the energy equation. The heat flux based on Newton's law of cooling is assumed as

$$q = H(T_{oc} - T_w), \qquad (46)$$

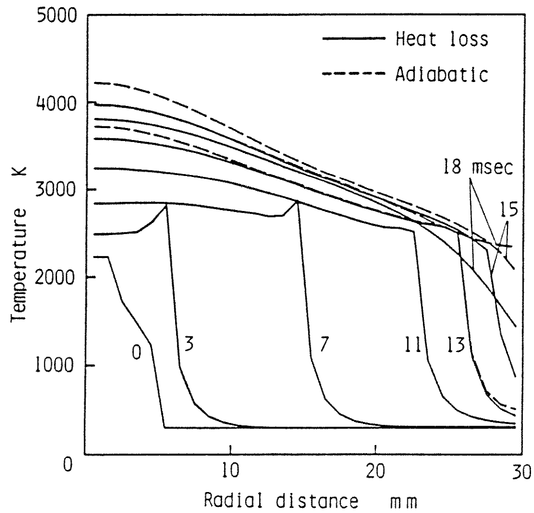

Fig. 17. Temperature distribution considering the effect of heat loss. Heat transfer coefficient: 0.6 MJ/(m^2 sec K).

where the wall temperature, T_w, is assumed to be independent of time, namely constant. In Figs. 16 and 17, the result which is obtained when H = 0.6 MJ/(m^2 sec K) is shown, where for comparison the result of the adiabatic case is also shown. In Fig. 16, it is shown that the agreement between the calculated and experimental result is perfect in this case.

RECTANGULAR TWO-DIMENSIONAL MODEL

By using a two-dimensional model, a simulation was tried of the flame propagation, which initiates from the center, in a cylindrical combustion chamber. The model in this case consists of two-dimensional, unsteady equations for the conservation of mass, momentum and energy for a reactive mixture of perfect gases. Equations, the computation procedure, the initial and boundary conditions and the experimental procedure are similar to those described in the spherical one-dimensional model except for following.

Model Description

The two-dimensional model was made on a laminar flame propagation through a stoichiometric propane-air mixture within a cylindrical combustion chamber of 60 mm in diameter and 16 mm in thickness. In this case, Eqs. (1) through (10) for the spherical one-dimensional model are replaced by the following equations.

Mass conservation.

$$\frac{\partial \rho}{\partial t} + \frac{\partial \rho u}{\partial x} + \frac{\partial \rho v}{\partial y} = 0 \quad (47)$$

Momentum conservation.

$$\frac{\partial \rho u}{\partial t} + \frac{\partial \rho u^2}{\partial x} + \frac{\partial \rho uv}{\partial y} = -\frac{\partial p}{\partial x} + \frac{\partial \sigma_{xx}}{\partial x} + \frac{\partial \sigma_{yx}}{\partial y} \quad (48)$$

$$\frac{\partial \rho v}{\partial t} + \frac{\partial \rho uv}{\partial x} + \frac{\partial \rho v^2}{\partial y} = -\frac{\partial p}{\partial y} + \frac{\partial \sigma_{xy}}{\partial x} + \frac{\partial \sigma_{yy}}{\partial y} \quad (49)$$

Energy conservation.

$$\frac{\partial \rho e_t}{\partial t} + \frac{\partial \rho e_t u}{\partial x} + \frac{\partial \rho e_t v}{\partial y} = -\frac{\partial pu}{\partial x} - \frac{\partial pv}{\partial y} + \frac{\partial}{\partial x}(\sigma_{xx}u + \sigma_{xy}v) + \frac{\partial}{\partial y}(\sigma_{yx}u + \sigma_{yy}v) - \frac{\partial q_x}{\partial x} - \frac{\partial q_y}{\partial y} + q_c \quad (50)$$

Species conservation.

$$\frac{\partial \rho_i}{\partial t} + \frac{\partial \rho_i u}{\partial x} + \frac{\partial \rho_i v}{\partial y} = \frac{\partial}{\partial x}\left(\rho D\frac{\partial Y_i}{\partial x}\right) + \frac{\partial}{\partial y}\left(\rho D\frac{\partial Y_i}{\partial y}\right) + (\rho_i)_c \quad (51)$$

Equation of state.

$$p = \rho RT \quad (52)$$

Miscellaneous.

$$\sigma_{xx} = 2\mu\frac{\partial u}{\partial x} + \lambda\left(\frac{\partial u}{\partial x} + \frac{\partial v}{\partial y}\right) \quad (53)$$

$$\sigma_{xy} = \sigma_{yx} = \mu\left(\frac{\partial u}{\partial y} + \frac{\partial v}{\partial x}\right) \quad (54)$$

$$\sigma_{yy} = 2\mu\frac{\partial v}{\partial y} + \lambda\left(\frac{\partial u}{\partial x} + \frac{\partial v}{\partial y}\right) \quad (55)$$

$$q_x = -\kappa\frac{\partial T}{\partial x} - h\sum_{i=1}^{n}\rho_i D\frac{\partial Y_i}{\partial x} \quad (56)$$

$$q_y = -\kappa\frac{\partial T}{\partial y} - h\sum_{i=1}^{n}\rho_i D\frac{\partial Y_i}{\partial y} \quad (57)$$

$$h = e + \frac{p}{\rho} \quad (58)$$

$$e_t = e + \frac{1}{2}(u^2 + v^2) \quad (59)$$

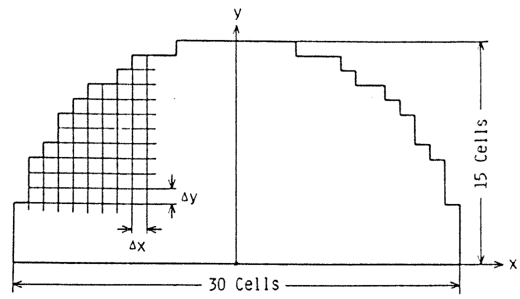

Fig. 18. Grid approximation of the combustion chamber.

The combustion chamber is divided into 450 square cells as show in Fig. 18. The size of the each cell is 2 x 2 mm. In order to save the computing time, the calculation was done on the semicircle which is shown in Fig. 18. Figure 19 shows the structure of the combustion chamber used in the experiment. In the numerical treatment, velocities as well as momentum were evaluated at the boundary between cells, while the other physical properties were done at the center of the cell as shown in Fig. 20.

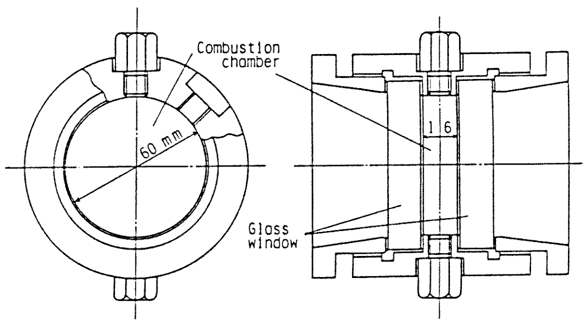

Fig. 19. Cylindrical combustion chamber.

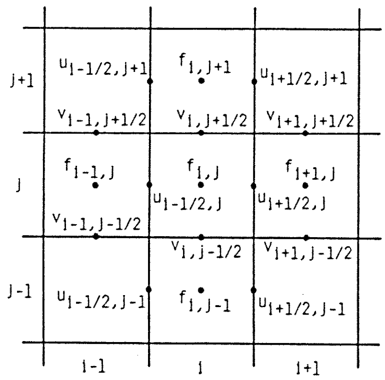

Fig. 20. Velocity (u and v) and the other physical property (f) in the cell arrangement.

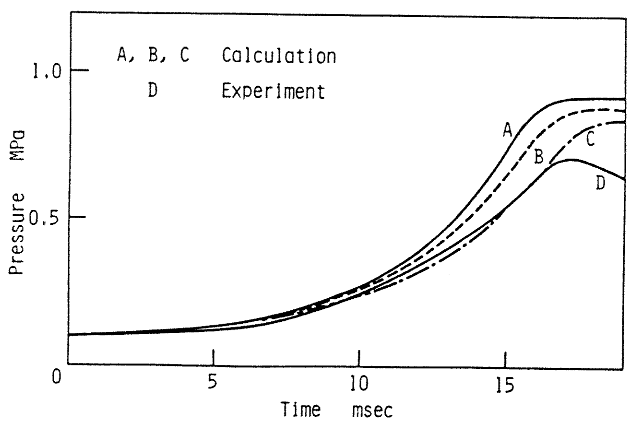

Fig. 21. Pressure vs. time in cylindrical combustion chamber. A; adiabatic: B and C; heat loss considered (H = 0.08 and 0.16 MJ/(m^2 sec K), respectively).

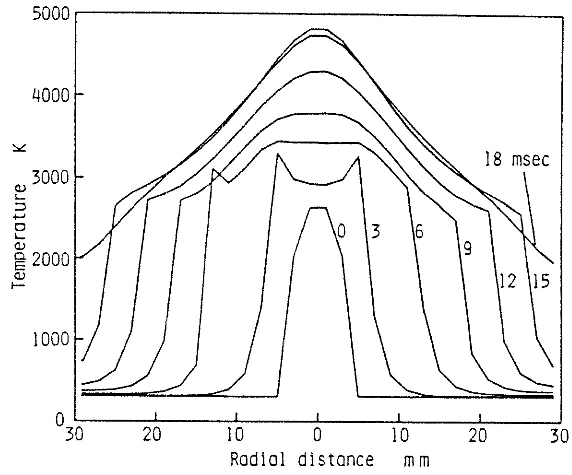

Fig. 22. Calculated temperature distribution in cylindrical combustion chamber under adiabatic condition.

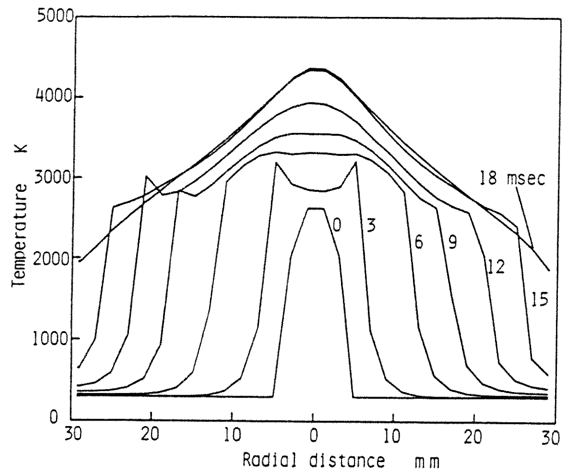

Fig. 23. Temperature distribution in cylindrical combustion chamber. Heat loss: H = 0.08 MJ/(m^2 sec K)

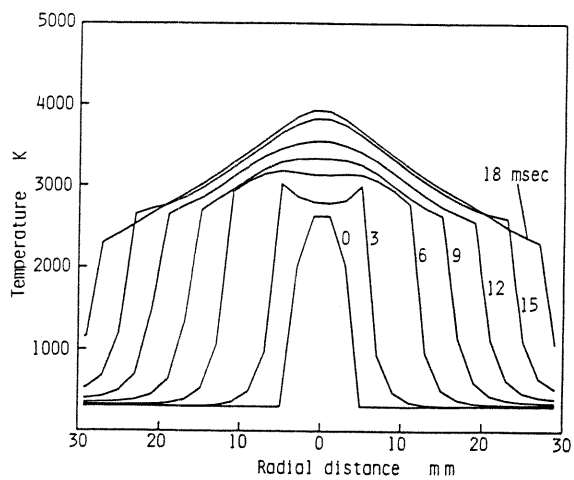

Fig. 24. Temperature distribution in cylindrical combustion chamber. Heat loss: H = 0.16 MJ/(m^2 sec K)

Results and Discussion

In calculation, the values of the parameters were used by which the best agreement between the calculated and experimental results had been obtained for the spherical one-dimensional model; namely 2.045 MJ/mol, 40 $m^3/(mol\ sec)$ and $1.9 \times 10^{-3}\ m^2/sec$ for the values of the heat of combustion, the pre-exponential factor and the diffusion coefficient, respectively. The calculated results are shown in Figs. 21-30.

In Fig. 21, the adiabatic, calculated curve is found to deviate from the experimental curve at earlier time than the aforementioned result in the spherical combustion chamber. This deviation is naturally caused by the fact that the flame front is in contact with the window glass from the early time to the end of the flame propagation. Therefore, heat loss from all the cells was taken into consideration. The results are shown in Fig. 21. As can be seen, in contrast to the results for the spherical system mentioned above, the agreement between the calculated and experimental results is not excellent. Strictry speaking, if two different heat transfer coefficients, namely for heat loss to the window glass and the circumferential wall which is made of Al alloy are considered, the discrepancy as shown in Fig. 21 may be reduced to a certain extent, but it does not seem to be essential.

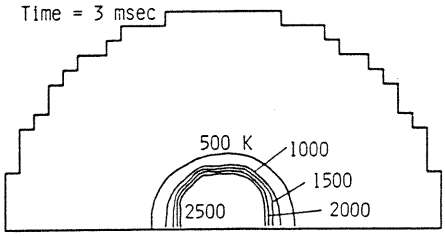

Fig. 25. Calculated isotherms under adiabatic condition.

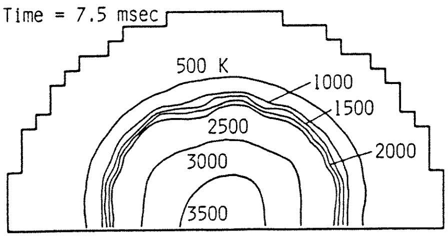

Fig. 26. Calculated isotherms under adiabatic condition.

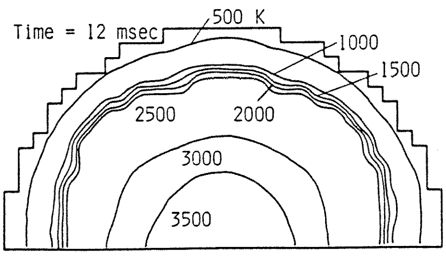

Fig. 27. Calculated isotherms under adiabatic condition.

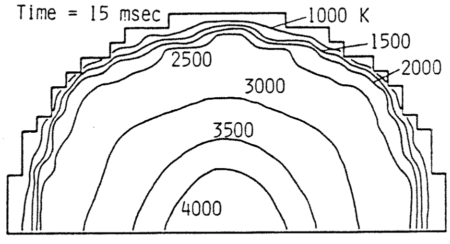

Fig. 28. Calculated isotherms under adiabatic condition.

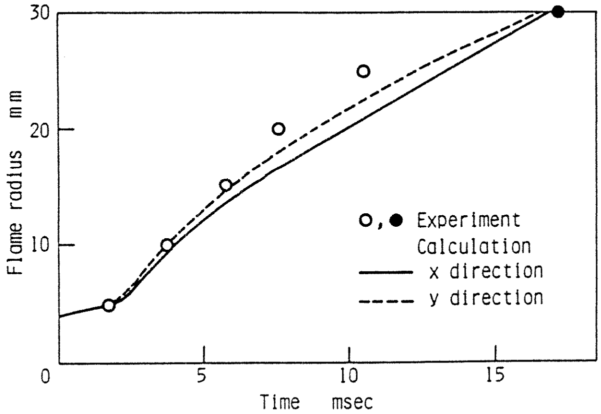

Fig. 29. Flame radius vs. time, comparison being made between experimental and calculated results.

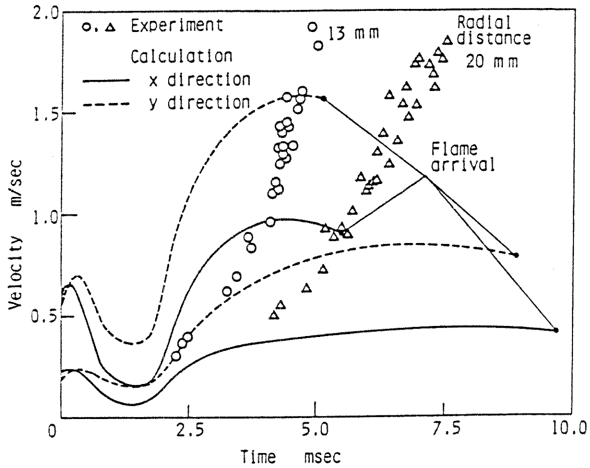

Fig. 30. Velocity change at the point of radial distance of 13 and 20 mm till flame arrival.

In Figs. 25-28, it is indicated that there exist some irregularities on the isotherms. This is due to a considerably larger size of cells. In these figures, it is also found that the flame speed is not the same towards x and y directions. This is caused by the sequence of the calculation of the finite difference equations and the discrepancy found between two directions may be reduced if a smaller cell size is used.

In Figs. 29 and 30, it is found that the agreement between the calculated and experimental results is not excellent, and that there exists disagreement in the flame radius and the unburned gas velocity in x and y directions.

CONCLUDING REMARKS

A modeling of one-dimensional spherical coordinate was developed for the flame propagation with central ignition, in the spherical combustion chamber. The optimum value of the parameters used in the model was decided by comparing the results obtained by the numerical calculation with the experimental result. The heat loss to the chamber wall was also considered in a simple manner. As results, agreement between calculated and experimental results is excellent in terms of the pressure of the combustion chamber, the position of the flame front and the gas velocity. However, the temperature calculated is higher than probable. This is caused by an employment of only one chemical reaction equation. Since the temperature is very sensitive to the pollutant formation, especially NO_x, there is room for further improvement; for example by using dissociation equation of carbon dioxide into carbon monoxide.

Next, by use of the values of the parameters which was decided in the aforementioned simulation of one-dimensional spherical flame propagation, a modeling of two-dimensional rectangular coordinates was tried for the flame propagation in the cylindrical combustion chamber with central ignition. The agreement of the calculated result with the experimental one is not so good compared with that for the spherical flame propagation. This mainly originates in too simple consideration of the heat loss used in the model. In order to introduce the heat loss effect properly into the model, three-dimensional model which dose not lengthen the computing time very much is most effective.

NOMENCLATURE

A = pre-exponential factor, $m^3/(mol\ sec)$
a = order of reaction
b = order of reaction
C = constant
C_p = heat capacity at constant pressure, J/(kg K)
C_v = heat capacity at constant volume, J/(kg K)
D = diffusion coefficient, m^2/sec
E = activation energy, J/mol
e = specific internal energy, J/kg
H = heat transfer coefficient, $J/(m^2\ K\ sec)$
h = specific enthalpy, J/kg
k = reaction rate constant, $m^3/(mol\ sec)$
M = molecular mass, kg/mol
m = mass, kg
p = pressure, Pa
Q = heat of combustion, J/mol of fuel
q = energy flux, $J/(m^2\ sec)$
$\dot{q}$ = heat release rate, $J/(m^3\ sec)$
R = gas constant, J/(kg K)
$\bar{R}$ = universal gas constant, J/(mol K)
r = radial coordinate, m
S = speed, m/sec
T = temperature, K
t = time, sec
u = velocity, m/sec
V_c = volume of combustion chamber, m^3
v = velocity, m/sec
x = rectangular coordinate, m
Y = mass fraction
y = rectangular coordinate, m
Δx, Δy = cell size, m
α = thermal diffusivity, m^2/sec
δ = thickness of flame front, m
κ = thermal conductivity, J/(m sec K)
λ = viscosity ($=-2\mu/3$), kg/(m sec)
μ = viscosity, kg/(m sec)
ρ = density, kg/m^3
$\dot{\rho}$ = production rate, $kg/(m^3\ sec)$
σ = stress tensor, Pa
ω = reaction rate, $mol/(m^3\ sec)$

Subscripts
b = burned
c = chemical reaction
C_3H_8 = propane
i = species
N_2 = nitrogen
O_2 = oxygen
oc = outer cell
Prod. = combustion product
r = radius
t = total
u = unburned
x = rectangular coordinate
y = rectangular coordinate
θ = angle in spherical coordinates
ϕ = angle in spherical coordinates

ACKNOWLEDGEMENT

We are indebted to Professor F. J. Weinberg of Imperial College, London for his giving us an opportunity to write the manuscript. This work was partly supported by a Grant in Aid for Special Project Research from the Ministry of Education, Science and Culture of Japan.

REFERENCES

1. Gupta, H. C., Steinberger, R. L. and Bracco, F. V., "Combustion in a Divided Chamber, Stratified Charge, Reciprocating Engine: Initial Comparisons of Calculated and Measured Flame Propagation," Combustion Science and Technology, Vol. 22, pp. 27-61, 1980.
2. Bracco, F. V. and O'Rourke, P. J., "A REVIEW OF INITIAL COMPARISONS OF COMPUTED AND MEASURED TWO-DIMENSIONAL UNSTEADY FLAME FIELDS," Progress in Energy and Combustion Science, Vol. 7, pp. 103-124, 1981.
3. Kono, M., Kumagai, S. and Sakai, T., "THE OPTIMUM CONDITION FOR IGNITION OF GASES BY COMPOSITE SPARKS," Sixteenth Symposium (International) on Combustion, The Combustion Institute, pp. 757-766, 1977.
4. Kono, M., Iinuma, K., Kumagai, S. and Sakai, T., "Spark Discharge Characteristics and Ignition Ability of Capacitor Discharge Ignition Systems," Combustion Science and Technology, Vol. 19, pp. 13-18, 1978.
5. Rivard, W. C., Farmer, O. A. and Butler, T. D., RICE: A Computer Program for Multicomponent Chemically Reactive Flows at All Speeds, Los Alamos Scientific Laboratory Report LA-5812, 1974.
6. Gupta, H. C. and Syed, S. A., "REC-P3: A Computer Program for Combustion in Reciprocating Engines," MAE Report No. 1431, Princeton University, 1979.